Dual Pressure versus Hybrid Recuperation in an Integrated Solid Oxide Fuel Cell Cycle – Steam Cycle

Rokni, Masoud

Published in:
Journal of Energy and Power Engineering

Publication date:
2014

Document Version
Publisher's PDF, also known as Version of record

Journal of Energy and Power Engineering 8 (2014) 596-611

Dual Pressure versus Hybrid Recuperation in an Integrated Solid Oxide Fuel Cell Cycle—Steam Cycle

Masoud Rokni

Department of Mechanical Engineering, Technical University of Denmark, Lyngby 2800, Denmark

Received: November 26, 2012 / Accepted: April 22, 2013 / Published: April 30, 2014.

Abstract: A SOFC (solid oxide fuel cell) cycle running on natural gas was integrated with a ST (steam turbine) cycle. The fuel is desulfurized and pre-reformed before entering the SOFC. A burner was used to combust the remaining fuel after the SOFC stacks. The off-gases from the burner were used to produce steam in a HRSG (heat recovery steam generator). The bottoming steam cycle was modeled with two configurations: (1) a simple single pressure level and (2) a dual pressure level with both a reheat and a pre-heater. The SOFC stacks in the present SOFC-ST hybrid cycles were not pressurized. The dual pressure configuration steam cycle combined with SOFC cycle (SOFC-ST) was new and has not been studied previously. In each of the configuration, a hybrid recuperator was used to recovery the remaining energy of the off-gases after the HRSG. Thus, four different plants system setups were compared to each other to reveal the most superior concept with respect to plant efficiency and power. It was found that in order to increase the plant efficiency considerably, it was enough to use a single pressure with a hybrid recuperator instead of a dual pressure Rankine cycle.

Key words: SOFC, fuel cell, hybrid cycle, steam cycle, Rankine cycle, hybrid recuperation.

1. Introduction

The solid oxide fuel cell is an electrochemical reactor currently under development by some companies to be used in future power and heat generation applications. Depending on the type of the electrolyte, they are working at temperature levels more than about 750 °C up to 1,000 °C. The lower temperature alternative is now being developed for market entry during this decade by, e.g., Topsoe fuel cells. Due to cost and material complications in the surrounding components some companies are trying to find new materials for the SOFC (solid oxide fuel cell) cells to decrease their operating temperature. Temperatures of about 650 °C have also been mentioned.

SOFC-based power plants have been studied for a while and some companies, such as Wärtsilä, are trying to realize such systems for CHP (combined heat and power) applications [1]. The SOFC plant is also combined with CC (combined cycles) in the literature to achieve ultra-high electrical efficiencies [2, 3]. Due to the current operating temperature of the SOFC stacks (more than about 750 °C), hybrid SOFC and GT (gas turbine) systems have been extensively studied in the literature, e.g., in Ref. [4] for CHP and in Refs. [5, 6] with internal biomass gasification. The characterization, quantification and optimization of hybrid SOFC-GT systems have been studied by Subramanyan and Calise et al. [7, 8]. The dynamics and control concept of a pressurized SOFC-GT hybrid system have also been studied, such as in Ref. [9]. In Ref. [10], modeling results are compared with measured data for a 220 kW hybrid SOFC-GT power plant. Details of the design, dynamics, control and startup of such hybrid power plants are studied in Ref. [11]. Part-load characteristics of a SOFC-micro GT were also studied in Ref. [12].

Corresponding author: Masoud Rokni, associate professor, research fields: hybrid fuel cell systems, integrated gasification and SOFC plants. E-mail: MR@mek.dtu.dk.

Despite extensive investigation on hybrid SOFC-GT plants by many researchers, the studies on combined SOFC-ST (steam turbine) are very limited [13-15]. In addition, the SOFC manufactures are trying to decrease the operating temperature of the SOFC stacks, which means that the combination of a SOFC-ST hybrid system would be more attractive than SOFC-GT systems. Decreasing the operating temperature will result in less material cost for the SOFC stacks which in turn results in that some problems associated with BoP (balance of plants) components will be diminished.

The current manuscript differs considerably from the previous studies in the sense that in the previous investigations the SOFC plant is pressurized, regardless the combinations (SOFC-GT, SOFC-CC or SOFC-GT-ST). However, in the current study the SOFC plant is not pressurized and it is working under ambient pressure. The compressor in the SOFC plants provides the necessary mass flow and pressure to compensate the pressure drops in the components (heat exchangers, SOFC stacks and burner) along the path of the air. The provided pressure by the compressor is about 1.2 bars for all cases considered. Thus technologically, the current hybrid systems are completely different from the previous suggested systems. This is another advantage of hybrid SOFC-ST systems compared to the SOFC-GT and SOFC-CC studies. In all the previous studies, the SOFC stacks must be pressurized in a large pressurized vessel (depending on the size of the plant) which brings up complicated practical problems.

In the bottoming Rankine cycle, a dual pressure level with reheat and pre-heater were used in this study. This was done because as known, in combined cycles (GT-ST) dual pressure levels with reheat and pre-heater are economical with respect to higher plant efficiency compared to a single pressure level. Thus, the results from a dual pressure Rankine cycle in combined SOFC-ST hybrid plants were compared with the corresponding results obtained from a single pressure Rankine cycle, in terms of plant efficiency and plant power. In addition, a hybrid recuperator was also used here to preheat the air prior to the cathode pre-heater of the SOFC plant in accordance to what was proposed in Ref. [14]. This was done for both single and dual pressure bottoming cycles to study the effect of hybrid recuperator versus dual pressure Rankine cycle in combined SOFC-ST plants. Such hybrid recuperator was shown to be very efficient and could increase the plant efficiency significantly. Thus, four different plants configurations were compared with each other in terms of plant efficiency and generated net power. Furthermore, hybrid recuperator versus dual pressure steam cycle was compared in terms of plant characterization.

It should be noted that the combination of a SOFC-ST cycle with dual pressure level in the steam cycle investigated here is new and has not been studied previously by the author. It should also be noted that the system presented here was studied thermodynamically and the objective of this study was not to present or discuss associated costs. The current investigation is regarded as a continuation study presented in Ref. [14]. The thermodynamic assessment is conducted by use of mathematical models describing the process which in turn relies on connecting zero-dimensional component models to generate a complete system model.

2. Methodology

The results of this paper were obtained using the in-house simulation tool called as DNA (dynamic network analysis) [16], which is a simulation tool for energy system analysis. It is the present result of an ongoing development at the Department of Mechanical Engineering, Technical University of Denmark, which began with a master's thesis work in Ref. [17]. Since then the program has been developed to be generally applicable covering unique features and hence supplementing other simulation programs.

In DNA, the physical model is formulated by

connecting the relevant component models through nodes and by including operating conditions for the complete system. The physical model is converted into a set of mathematical equations to be solved numerically. The mathematical equations include mass and energy conservation for all components and nodes as well as relations for thermodynamic properties of the fluids involved. During the development of DNA, the four key terms portability, robustness, efficiency, and flexibility were kept in mind as the important features for making a generally applicable tool for energy system studies. The program is written in FORTRAN.

2.1 Modeling of SOFC Stacks

The SOFC model used in this investigation is based on the planar type developed by DTU-Risø and TOPSØE Fuel Cell. The model was calibrated against experimental data in the range of 650 °C to 800 °C (SOFC operational temperature) as described and implemented in Refs. [14, 18]. For the sake of clarification, it is shortly described here. The model is assumed to be a zero-dimensional, thus enabling calculation of complicated energy systems. In such modeling one must distinguish between electrochemical modeling, calculation of cell irreversibility (cell voltage efficiency) and the species compositions at outlet. The operational voltage (E_{FC}) was found to be:

$$E_{FC} = E_{Nernst} - \Delta E_{act} - \Delta E_{ohm} - \Delta E_{conc} - \Delta E_{offset} \quad (1)$$

where, E_{Nernst}, ΔE_{act}, ΔE_{ohm}, ΔE_{conc} and ΔE_{offset} are the Nernst ideal reversible voltage (open voltage circuit), activation polarization, ohmic polarization, concentration polarization and the offset polarization, respectively. The offset polarization is neglected and assuming that only hydrogen is electrochemically converted, then the Nernst equation can be written as:

$$E_{Nernst} = \frac{-\Delta \bar{g}_f^0}{n_e F} + \frac{RT}{n_e F} \ln\left(\frac{p_{H_2,tot}\sqrt{p_{O_2}}}{p_{H_2O}}\right) \quad (2)$$

$$p_{\mathrm{H2,tot}} = p_{\mathrm{H2}} + p_{\mathrm{CO}} + 4p_{\mathrm{CH_4}} \quad (3)$$

where, Δg_f^0 is the Gibbs free energy (for H_2 reaction) at standard pressure. The water-gas shift reaction is very fast and therefore the assumption of hydrogen as only species to be electrochemically converted is justified [19, 20]. In the above equations p_{H2} and p_{H2O} are the partial pressures for H_2 and H_2O, respectively. The partial pressures were assumed to be the average between the inlet and outlet weighted by molar fraction (y) for anode and cathode separately as:

$$p_j = \left(\frac{y_{j,\mathrm{out}} - y_{j,\mathrm{in}}}{2}\right) p_{anode}$$

$$j = \{\mathrm{H_2, CO, CH_4, CO_2, H_2O, N_2}\} \quad (4)$$

$$p_{\mathrm{O_2}} = \left(\frac{y_{\mathrm{O_2,out}} - y_{\mathrm{O_2,in}}}{2}\right) p_{\mathrm{cathode}}$$

The change in standard Gibbs free energy ($\Delta \bar{g}_f^{\,0}$) was for H_2 reaction and the number of electrons transferred for each molecule of fuel (n_e = 2) and was calculated by:

$$\Delta \bar{g}_f^0 = \left(\bar{g}_f^0\right)_{H_2O} - \left(\bar{g}_f^0\right)_{H_2} - \frac{1}{2}\left(\bar{g}_f^0\right)_{O_2} \quad (5)$$

The activation polarization was evaluated from the Butler-Volmer equation [21] by isolating it from other polarizations to determine the charge transfer coefficients and exchange current density from the experiment by the curve fitting technique.

The ohmic polarization depends on the electrical conductivity of the electrodes as well as the ionic conductivity of the electrolyte. This was also calibrated against experimental data for a cell with anode thickness, electrolyte thickness and cathode thickness of 600, 50 and 10 μm, respectively.

The concentration polarization is dominant at high current densities for anode-supported SOFCs, wherein insufficient amounts of reactants are transported to the electrodes and the voltage is then reduced significantly. It was modeled as function of diffusion coefficient, anode limiting current and current density. The anode limiting current was modeled as function of anode porosity, anode tortuosity and a binary diffusion coefficient. Both diffusion coefficient and the binary diffusion coefficient were calibrated against experimental data [22].

The fuel composition at anode outlet was calculated using the Gibbs minimization method as described in Ref. [23]. Equilibrium at the anode outlet temperature and pressure was assumed for the following species: H_2, CO, CO_2, H_2O, CH_4 and N_2. Thus, the Gibbs minimization method calculates the compositions of these species at outlet by minimizing their Gibbs energy. The equilibrium assumption is fair because the methane content in this study is very low.

Finally, the current density is directly proportional to the amount of reacting hydrogen and the cell area, according to Faraday's law. The fuel composition leaving the anode was calculated by the Gibbs minimization method. The power production from the SOFC (P_{SOFC}) depends on the amount of chemical energy fed to the anode, the reversible efficiency (η_{rev}), the voltage efficiency (η_v) and the fuel utilization factor (U_F). It is defined in mathematical form as:

$$P_{SOFC} = \eta_{rev}\,\eta_v\,U_F \begin{pmatrix} LHV_{H_2}\dot{n}_{H_2,in} \\ +LHV_{CO}\,\dot{n}_{CO,in} \\ +LHV_{CH_4}\,\dot{n}_{CH_4,in} \end{pmatrix} \tag{6}$$

where, $\dot{n}$ was the molar reaction rate (molar flow), U_F was a set value and η_v was defined as:

$$\eta_v = \frac{\Delta E_{\text{cell}}}{E_{Nernst}} \tag{7}$$

The reversible efficiency is the maximum possible efficiency defined as the relationship between the maximum electrical energy available (change in Gibbs free energy) and the fuels LHV (lower heating value) as follows [24]:

$$\eta_v = \frac{E_{\text{cell}}}{E_{Nernst}} \tag{8}$$

$$\eta_{rev} = \frac{\left(\Delta\bar{g}_f\right)_{fuel}}{LHV_{fuel}} \tag{9}$$

$$\begin{aligned} \left(\Delta\bar{g}_f\right)_{fuel} = &\left[\left(\bar{g}_f\right)_{H_2O} - \left(\bar{g}_f\right)_{H_2} - \frac{1}{2}\left(\bar{g}_f\right)_{O_2}\right] y_{H_2,in} \\ &+\left[\left(\bar{g}_f\right)_{CO_2} - \left(\bar{g}_f\right)_{CO} - \frac{1}{2}\left(\bar{g}_f\right)_{O_2}\right] y_{CO,in} \\ &+\left[\begin{matrix}\left(\bar{g}_f\right)_{CO_2} + 2\left(\bar{g}_f\right)_{H_2O} \\ -\left(\bar{g}_f\right)_{CH_4} - 2\left(\bar{g}_f\right)_{O_2}\end{matrix}\right] y_{CH_4,in} \end{aligned} \tag{10}$$

2.2 Modeling of Fuel Pre-reforming

A Gibbs reactor is used in this study, meaning that the total Gibbs free energy has its minimum when the chemical equilibrium is achieved. Such characteristic can be used to calculate the gas composition at a specified temperature and pressure without considering the reaction pathways. The Gibbs free energy of a gas (assumed to be a mixture of k perfect gases) is given by:

$$\dot{G} = \sum_{i=1}^{k} \dot{n}_i \left[g_i^0 + RT\,\ln\left(y_i\,p\right)\right] \tag{11}$$

where, g^0, R, T and y_i are the specific Gibbs free energy, universal gas constant, gas temperature and molar fraction, respectively. Each atomic element in the inlet gas is in balance with the outlet gas composition, which shows that the flow of each atom has to be conserved. For N elements, this balance is expressed as [23]:

$$\sum_{i=1}^{k} \dot{n}_{i,in}\,\mathbf{A}_{ij} = \sum_{m=1}^{w} \dot{n}_{m,out}\,\mathbf{A}_{mj}\,, \quad \text{for } j = 1,N \tag{12}$$

The N elements correspond to H, C and O in this pre-reforming process. A_{mj} is the number of atoms of element j (H, C, O, N) in each molecule of entering compound i (H_2, CH_4, CO, CO_2, H_2O, O_2, N_2 and Ar), while A_{ij} is the number of atoms of element j in each molecule of leaving compound m (H_2, CH_4, CO, CO_2, H_2O, N_2 and Ar). The minimization of the Gibbs free energy can be formulated by introducing a Lagrange multiplier, μ, for each of the N constraints obtained in Eq. (12). After adding the constraints, the expression to be minimized is then:

$$\phi = \dot{G}_{tot,out} + \sum_{j=1}^{N} \mu_j \left(\sum_{i=1}^{k} \dot{n}_{i,out}\,A_{ij} - \sum_{m=1}^{w} \dot{n}_{m,in}\,A_{mj}\right) \tag{13}$$

By setting the partial derivation of this equation with respect to $\dot{n}_{i,out}$ into zero then the function φ can be minimized as:

$$\begin{aligned} &\frac{\partial\varphi}{\partial\dot{n}_{i,out}} = \frac{\partial\dot{G}_{tot,out}}{\partial\dot{n}_{i,out}} + \sum_{j=1}^{N}\mu_j A_{ij} = 0 \quad \text{for } i = 1,k \\ &\Rightarrow\; g_{i,out}^0 + RT\ln\left(n_{i,out}\,p_{out}\right) + \sum_{j=1}^{N}\mu_j A_{ij} = 0 \\ &\text{for } i = 1,k \end{aligned} \tag{14}$$

2.3 Modeling of Other Components

The pumps power consumption was calculated as:

$$W_{pump} = \left[\frac{\dot{m} \upsilon_{in} (p_{out} - p_{in})}{\eta} \right]_{pump} \quad (15)$$

where, $\dot{m}$, p, υ and η were the mass flow, pressure, specific volume (m^3/kg) and efficiency of the pump, respectively. The pump efficiency and outlet pressure was defined as shown below. The power consumption for compressors were modeled based on the definition of isentropic and mechanical efficiencies (given values) as:

$$\eta_{is} = \left[\frac{h_{out,Sin} - h_{in}}{h_{out} - h_{in}} \right]_{compressor} \quad (16)$$

$$\eta_m = \left[\frac{\dot{m}(h_{out} - h_{in})}{W} \right]_{compressor} \quad (17)$$

where, h was the enthalpy for the corresponding state. Note also that h_{Sin} was the enthalpy when entropy was kept constant as for inlet.

In modeling a heat exchanger, it was assumed that all energy from one side is transferred to the other side if heat losses were neglected, (which was also the case in this study), as:

$$\dot{Q} = \dot{m}_1 (h_1 - h_2) \quad (18)$$

where, the subscript 1 and 2 referred side 1 and side of the heat exchanger. If pinch temperature was given then the minimum temperature was found at hot or cold end, or when a flow was changed between one- and two-phase as:

$$\Delta T_{\min} = \min\{T_{hot} - T_{cold}\} \quad (19)$$

The deaerator removes dissolved gasses and impurities from the condenser by keeping it in a reservoir at the state of a saturated liquid and with absorbing heat extracted from the steam turbine. Thus, in modeling, the outlet of feed water was assumed to be saturated in addition to the equations for mass and energy balance,

$$\sum \dot{m}_{in,dea} = \dot{m}_{out,dea} \quad (20)$$

$$\sum \dot{m}_{in,dea} h_{in,dea} = \dot{m}_{out,dea} h_{out,dea} \quad (21)$$

3. Plant Configurations

The plant configurations studied are shown in Figs. 1 and 2. Fig. 1a shows SOFC with single pressure level Rankine cycle while Fig. 1b (case A) shows SOFC with dual pressure level Rankine cycle (case B). Fig. 2 shows the same plant configurations in Fig. 1 but with when a HR (hybrid recuperator) is included. Fig. 2a is SOFC with single pressure Rankine cycle including hybrid recuperator (case C) and Fig. 2b shows SOFC with dual pressure Rankine cycle with hybrid recuperator (case D). Note that case A and C were already presented in Ref. [14], but in order to facilitate the compression they were also discussed in this investigation. The supplied NG (natural gas) is usually pressurized, and therefore no pump was used in the fuel line. The fuel was preheated in a fuel pre-heater heat exchanger before it was sent to a desulfurization unit wherein the sulfur content in the fuel was removed.

This unit was assumed to be a catalyst, operating at temperature of 200 °C. Thereafter, the desulfurized fuel was preheated in a pre-reformer heat exchanger to reach the operational temperature of the ASR (adiabatic steam reformer) catalyst, wherein the heavier hydrocarbons of the fuel were cracked down into the lighter ones. The pre-reformed fuel was now preheated in an AP (anode pre-heater) to 650 °C before being sent to the anode side of the SOFC stacks [11]. The operating temperature of the SOFC stacks and outlet temperatures were assumed to be 780 °C which is also assumed to be the outlets temperatures at both cathode and anode sides.

Therefore, the burned fuel after the stacks had a temperature of about 780 °C, which was used to preheat the fuel in the anode pre-heater. On the other side, air was compressed and then preheated in a CP (cathode pre-heater) to 600 °C before entering the cathode side of the SOFC stacks [11]. These entering temperatures are essential requirements for proper functioning of SOFC stacks, not only to initiate the

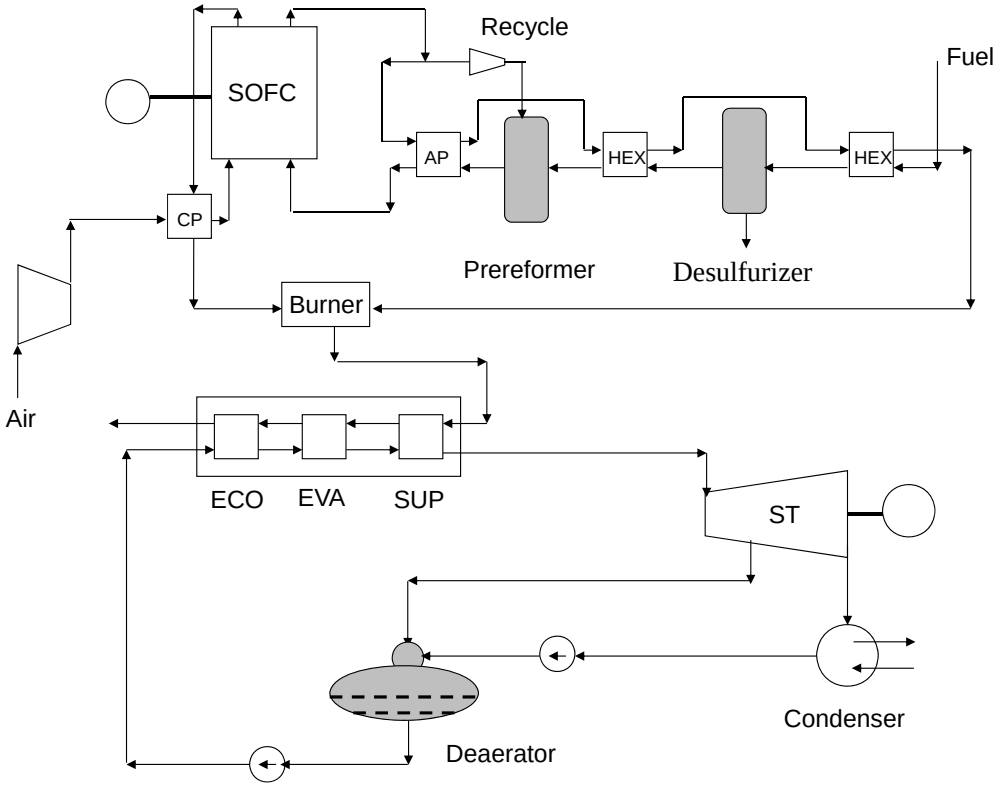

(a) Case A

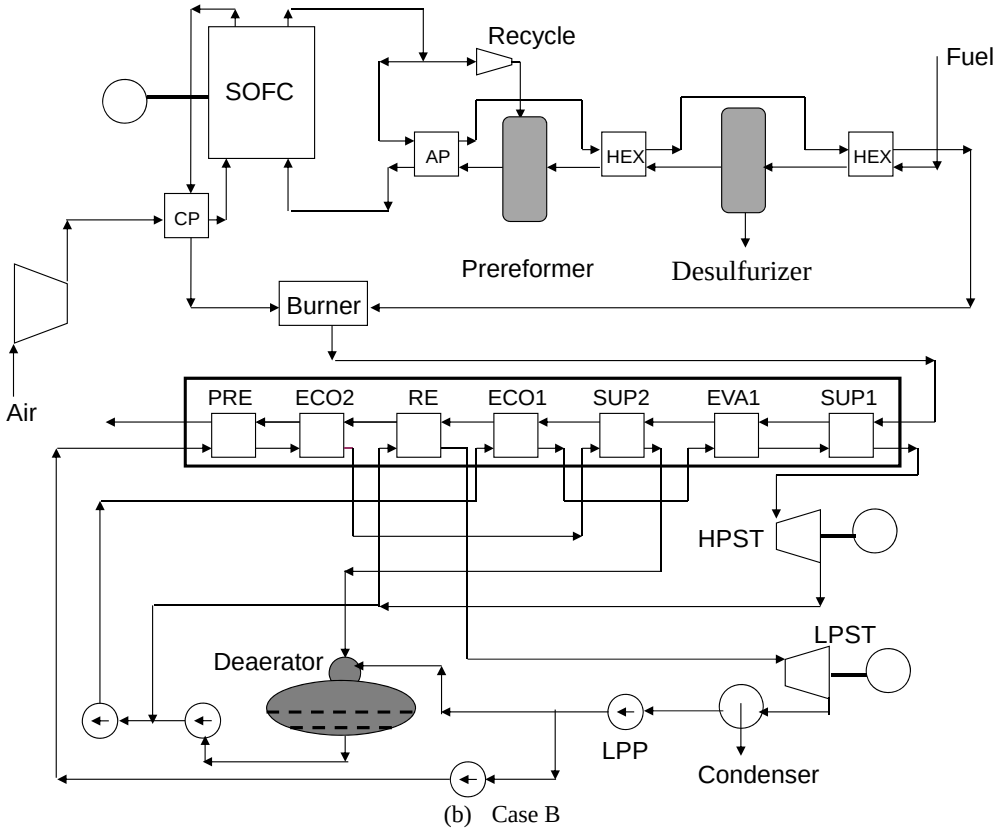

(b) Case B

Fig. 1 Combined SOFC-ST cycle plant without hybrid recuperator, (a) single pressure Rankine cycle and (b) dual pressure Rankine cycle.

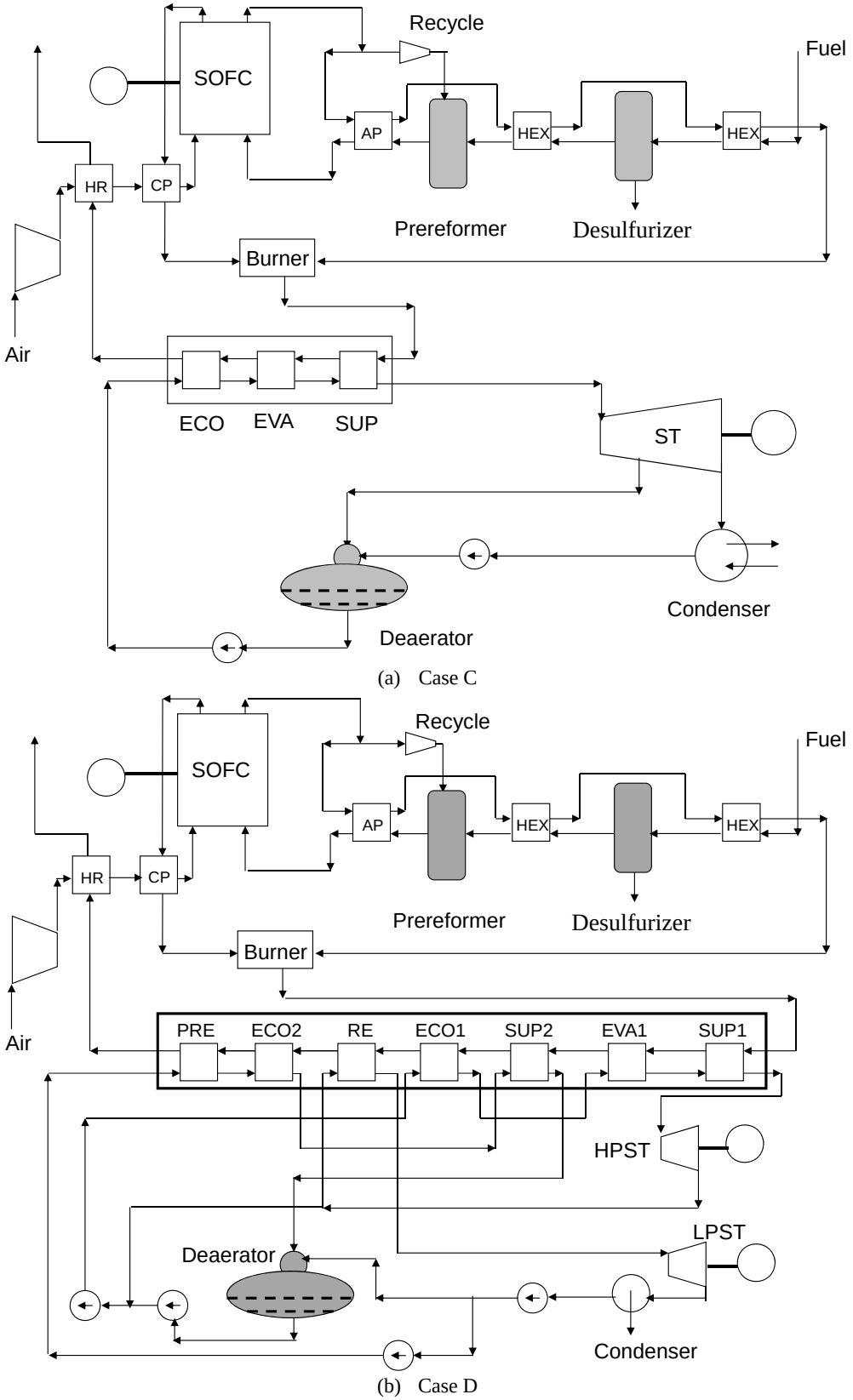

Fig. 2 Combined SOFC-ST plant with hybrid recuperator, (a) single pressure Rankine cycle and (b) dual pressure Rankine cycle.

chemical reactions but also for avoiding thermal fractures. Because the fuel in the SOFC stacks would not burn completely, the rest of the fuel together with the air coming out of the cathode side of the stacks were sent to a burner for further combustion. The off-gases from the burner had a high heat quality, which could be used to generate steam in a HRSG (heat recovery steam generator). Two types of Rankine cycle were used in this study: a single pressure level with deaerator (feed water tank) and a dual pressure level with reheat and pre-heater. In the single pressure level, the pressurized water after the feed water pump was superheated to steam in three stages: an ECO (economizer), an EVA (evaporator) and a SUP SUP (super)-heater. The generated steam was then expanded in a steam turbine to generate power. Part of the expanded steam was extracted for the deaeration. The expanded steam after the turbine was then cooled down in a condenser before pumping to the deaerator (Fig. 1a).

In the dual pressure level, more complicated setup was used; in the high pressure loop an ECO1 (economizer), an EVA1 (evaporator) and a SUP1 (super-heater) were used while in the low pressure loop PRE (a pre-heater), an ECO2 (economizer) and a SUP2 (super-heater) were used. Some of the steam after the HPST (high pressure steam turbine) was reheated in Fig. 1b and sent to LPST (low pressure steam turbine) as shown in Fig. 1b. It is worth to note that the presented dual pressure steam cycle as bottoming cycle for the SOFC cycle is novel and has not been studied in the open literature.

In Fig. 2, the energy of the off-gases from the HRSG was further utilized in a HR (hybrid recuperator) in the figure to preheat the air after the compressor of the SOFC cycle. In other words, heat was recycled back to the SOFC cycle. The study of Rokni [14] showed that such technique increases the plant efficiency significantly if a single pressure Rankine cycle was used as s bottoming cycle. However, such advantage is not known if a dual pressure Rankine cycle with reheat and pre-heater is used. The present study should reveal this issue.

As is known, an ASR reformer needs superheated steam for operation, which must be supplied to the reformer externally during start-up. However, during normal operation steam is available after the SOFC stacks due to the reactions of hydrogen and oxygen. Therefore, the stream after the anode side of SOFC was recycled using an ejector, as shown in Figs. 1 and 2.

4. Results and Discussions

For the sake of clarity, natural gas was defined as (in molar percentage):

CH_4: 0.87;

H_2S: 0.00375;

C_2H_6: 0.081;

CO_2: 0.02925;

C_3H_8: 0.01;

C_4H_{10}: 0.006.

The main parameters for the plant are shown in Table 1. The number of SOFC stacks was assumed to be 10,000 and number of cells per stacks was assumed to be 74. Furthermore, the utilization factor for the SOFC cells was assumed to be 0.8.

The pressure drops for all heat exchangers were assumed to 0.01 bars for air flow as well as steam flows, however, for fuel side it was assumed to be 0.005 bars. These values depend on the heat exchanger types and channel geometries, but they are reasonable for plate heat exchanger types with respect to flow their mass flow. The minimum temperature differences at pinch (ΔT_{min}) were assumed to be 30, 15 and 17 °C for the superheater, evaporator and economizer, respectively. Similar values were also assumed for the respective heat exchangers used in the dual pressure level. Thus for HRSG terminal temperature and pinch temperature were assumed to be 30 °C and 15 °C, respectively, while approach temperature was assumed to be 2 °C. By applying approach temperature one may avoid evaporation in the economizer when the plant is running on off-design. The SOFC stacks provide direct

Table 1 Main parameters for design point calculations of Figs. 1 and 2.

Parameter	Case A	Case B	Case C	Case D
Compressor inlet temperature (°C)	25	25	25	25
Compressor isentropic efficiency	0.85	0.85	0.85	0.85
Compressor mechanical efficiency	0.95	0.95	0.95	0.95
SOFC cathode inlet temperature (°C)	600	600	600	600
SOFC utilization factor	0.80	0.80	0.80	0.80
SOFC number of cells	74	74	74	74
SOFC number of stacks	10,000	10,000	10,000	10,000
SOFC cathode side pressure drop ratio (bar)	0.05	0.05	0.05	0.05
SOFC anode side pressure drop ratio (bar)	0.01	0.01	0.01	0.01
HEXes pressure drops (bar)	0.01	0.01	0.01	0.01
Fuel inlet temperature (°C)	25	25	25	25
Desulfurizer operation temperature (°C)	200	200	200	200
Pre-reformer inlet temperature (°C)	400	400	400	400
Pre-reformer outlet temperature (°C)	450	450	450	450
SOFC anode inlet temperature (°C)	650	650	650	650
SOFC operating temperature (°C)	780	780	780	780
Burner efficiency	0.98	0.98	0.98	0.98
HR~~SG~~ outlet temperature (°C)	-	-	90	90
Steam turbine isentropic efficiency	0.9	0.9	0.9	0.9
Extraction pressure	2	2	2	2
Second pressure level	-	3.49 bar	-	3.49
Condenser pressure	0.05 bar	0.05 bar	0.05 bar	0.05 bar
Pumps efficiency	0.85	0.85	0.85	0.85
Generators efficiency	0.97	0.97	0.97	0.97

Case A: single pressure level, without hybrid recuperator;
Case B: dual pressure level, without hybrid recuperator;
Case C: single pressure level, with hybrid recuperator;
Case D: dual pressure level, with hybrid recuperator.

current which needs to be converted to AC by using a converter. Such converters have an efficiency of about 97%-99% depending on the plant size, but such efficiency was neglected in the present study because their contribution on total plant efficiency and plant output is insignificant.

Extraction pressure in the single pressure Rankine cycle or second pressure level in the dual pressure one has a small effect on the plant efficiency and power output. Several calculations were carried out to find the optimal extraction pressure and second pressure level, but these calculations are not included in this study. As mentioned earlier the SOFC plant was not pressurized (unlike almost all previous investigations). Therefore, the pressure ratio for the compressor was not a set-point but could be calculated depending on the pressure drops in the following components. For example, the calculated pressure ratio in all cases considered here were less than 1.2 bars.

In each plant configuration, one needs to find the optimal live steam pressure in the bottoming cycle. Live steam pressure versus plants efficiencies for the case A and B were shown in Figs. 3a and 3b, respectively. As was evident, there existed a point at which the plant efficiency was maxima. For case A, the maximum plant efficiency occurred when the live steam pressure was at 22 bar (the solid-line). Note that the efficiency lines (η_{SOFC}, η_{ST} and η_{plant}) must be read on the left-hand side y-axis, while moisture line must be read from the right-hand side y-axis. For case B, the maximum plant efficiency occurred when the live steam pressure was at 43 bar. Another important issue

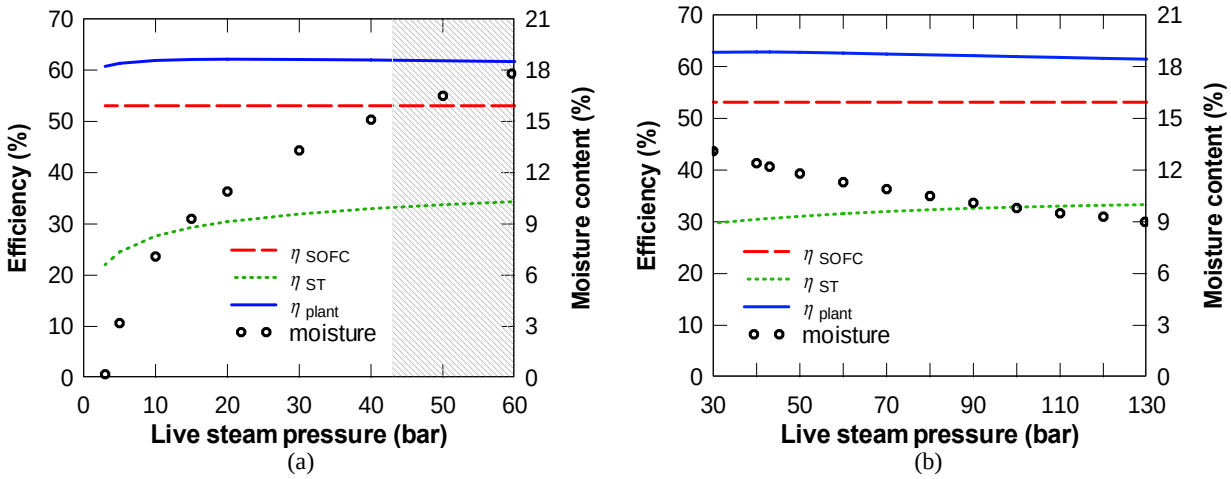

Fig. 3 Effect of live steam pressure on plants efficiencies and moisture content: (a) Case A; (b) Case B.

is the moisture content at the last stage of the steam turbine. Too high level of moisture (more than about 16%) may cause blade corrosion at the last stage [25]. For case A, the moisture content reached to 16% when live steam pressure was about 46 bar which was much higher than the maximum value (dot-line and right hand axis in Fig. 3a). Although, the optimal live steam pressure of 22 bar could be chosen for case A without concerning on moisture content at the last blade stage of the steam turbine.

The dashed area in Fig. 3a represents the area in which moisture content was above the limit value and therefore was not accepted here. For case B, the moisture content was well below the limit value and was decreasing with increasing live steam pressure.

Live steam pressure versus plants efficiencies for the cases C and D were shown in Fig. 4. For both case C and D, the plant efficiency increased when the live pressure increased (left-hand side y-axis). For case C, the moisture content reached to 16% when live steam pressure was about 103 bars. However, for case D, the moisture content was well below the limited value (right-hand side y-axis). For case D the calculations were stopped at 160 bars due to practical problems associated with designing of such steam turbine may occur at such pressures, mass flow and power output.

One may also conclude from Figs. 3 and 4 that moisture content problem occurs only for single pressure level while such problem did not exist for the dual pressure level configuration presented above.

Another conclusion from Figs. 3 and 4 was that for the cases without hybrid recuperation the topping cycle efficiency remained unchanged when the bottoming live steam pressure was changed (Fig. 3). However, this was not true for the cases with hybrid recuperations (Fig. 4). The SOFC cycle efficiency decreased somewhat with increasing live steam pressure. The reason was that the energy fed to the topping cycle was not only coming from the fuel itself but also was coming from the recuperated heat from the HRSG. Thus the efficiencies defined here are shown below:

$$\eta_{SOFC} = \frac{\text{Net power from SOFC cycle}}{\text{fuel consumption + recuperated heat}}$$

$$\eta_{ST} = \frac{\text{Net power from steam cycle}}{\text{heat into steam cycle through HRSG}} \qquad (22)$$

$$\eta_{plant} = \frac{\text{total net power hybrid plant}}{\text{fuel consumption}}$$

Furthermore, Figs. 3 and 4 showed that the steam cycle efficiency increased when the live steam pressure was increased, regardless of the case. This could not be discussed without presenting Figs. 5a and 5b, in which the effect of live steam pressure on plants net power output as well as HRSG effectiveness were shown. Note that the power lines (P_{SOFC}, P_{ST} and P_{plant}) must be read on the left-hand side y-axis, while HRSG effectiveness line must be read from the right-hand side y-axis.

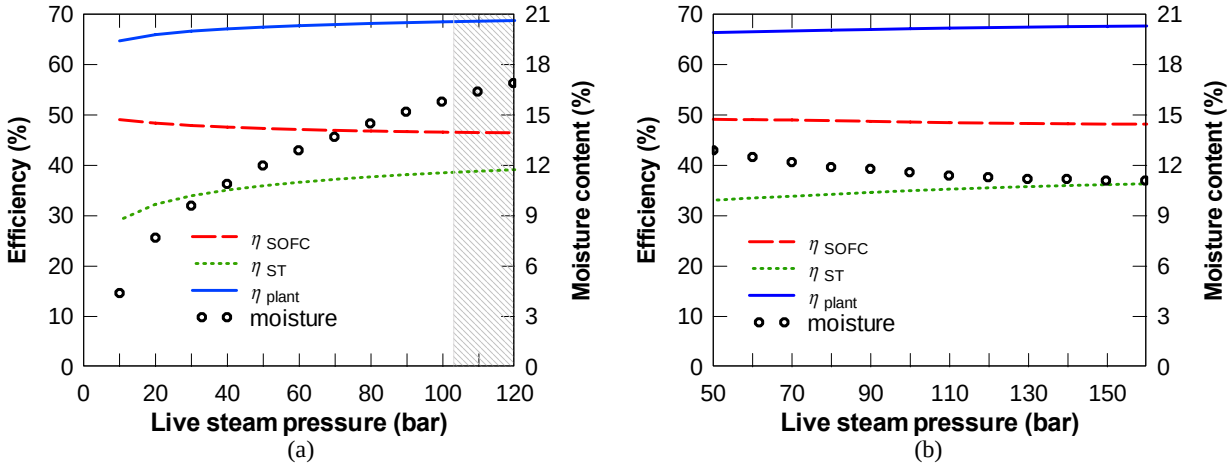

Fig. 4 Effect of live steam pressure on plants efficiencies and moisture content: (a) Case C; (b) Case D.

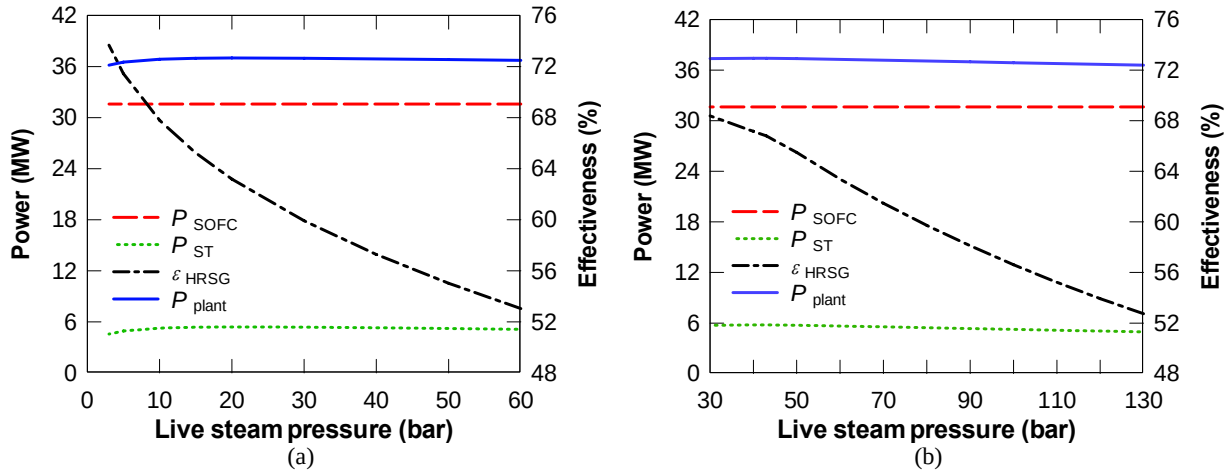

Fig. 5 Effect of live steam pressure on plants net power output and HRSG effectiveness: (a) Case A; (b) Case B.

Expanding steam at higher live steam pressure resulted in greater enthalpy drop over the turbine, which in turn resulted in higher steam turbine output. On the other hand, the evaporation temperature could be increased and therefore less steam could be generated (due to constant heat available from topping cycle). The effect of higher enthalpy drop may compensate the effect of lower steam mass flow to some extent, meaning that the net power output from steam turbine did not change significantly as showed in Fig. 5. However, generating steam at higher temperature resulted in much lower effectiveness of HRSG. Therefore, heat absorbed by the steam cycle was decreasing significantly and based on the definition (Eq. (22)), steam turbine efficiency was increased as shown in Figs. 3 and 4.

The effectiveness of the HRSG was defined as:

$$\varepsilon_{HRSG} = \frac{h_{HRSG,in} - h_{HRSG,out}}{h_{HRSG,in} - h_{air}} \tag{23}$$

which defined the ratio between the actual heat transfer and the maximum possible heat transfer in the HRSG.

For the hybrid recuperation cases the efficiency of the topping cycle was decreasing slightly when the live steam pressure was increased, meaning that the burner temperature was increased slightly and therefore steam could be produced at higher temperature. This in turn increased the enthalpy drop over steam turbine and consequently both efficiency and net power output of the bottoming cycle was increased slightly with increasing live steam pressure (Figs. 6a and 6b). The effectiveness of the HRSG was much higher than the

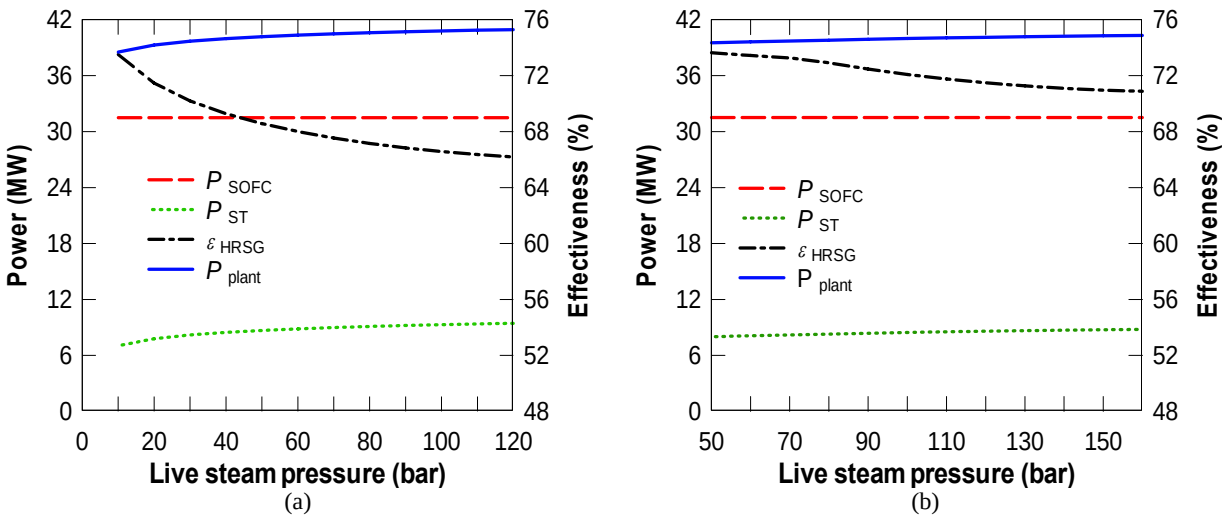

Fig. 6 Effect of live steam pressure on plants net power output and HRSG effectiveness: (a) Case C; (b) Case D.

non-hybrid recuperation cases which can be seen by comparing Fig. 5 with Fig. 6.

Due to corrosion problems, the off-gases could not be allowed to cool down to the ambient temperature and, therefore, the heat transfer was stopped at 90 °C. Note also that the power produced by the SOFC cycle did not change when live steam pressure was increased, neither in non-hybrid recuperating cases (case A and B) nor in hybrid recuperating cases (cases C and D). For the non-hybrid recuperating cases the net power produced in the plant had maximum because the netpower produced by the steam turbine had a maximum when live steam pressure was increased. This was due to the co-effect of enthalpy drop over the turbine and the amount of generated steam, as discussed above. For cases A and B the burner temperature remains unchanged when the live steam pressure is increased because the power produced by the SOFC cycle remains constant (Figs. 7a and 7b). Note that the heat line must be read on the left-hand side y-axis, while temperature lines (T_{burner} and T_{stack}) must be read from the right-hand side y-axis. Increasing live steam pressure resulted in generating steam at higher temperature which in turn decreased the HRSG effectiveness and therefore heat absorbed by the steam cycle was decreased as an effect. Consequently, the HRSG stack temperature (outlet temperature) was increasing. This was the basis to introduce the hybrid recuperator.

The idea of applying hybrid recuperating was not to increase the power produced in the topping cycle but to recover more energy from the HRSG and send it back to the steam cycle by increasing the temperature of the generated steam. The hybrid recuperator increased the energy supplied to the SOFC cycle which in turn decreased the duty of the cathode pre-heater. Therefore, more energy was left from the SOFC off-gases to be sent to the burner which in turn resulted in increasing the burner temperature and consequently increasing the temperature of the generated steam. Increasing live steam pressure resulted in increasing hybrid recuperating which in turn resulted in higher burner temperature as shown in Figs. 8a and 8b.

Heat absorbed by the steam cycle remains constant but the temperature of the generated steam increases. Note that the steam temperature was 30 °C lower than the off-gases temperature coming out from the burner (the HRSG terminal temperature mentioned above). Increasing generated steam temperature without changing the absorbed heat means that the exergy losses from the HRSG were decreased. This is an important issue to be mentioned and repeated again that the energy recovery from the HRSG through hybrid

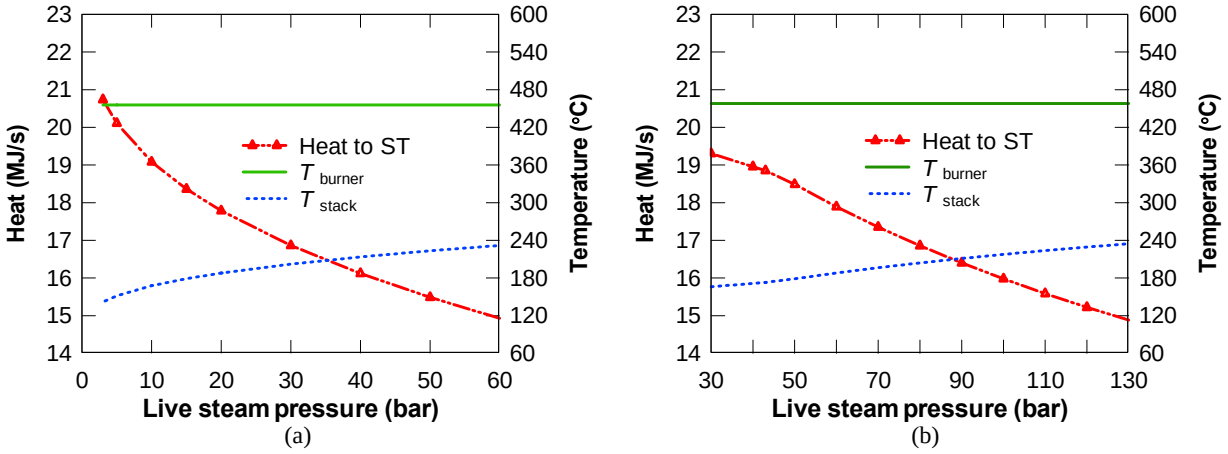

Fig. 7 Effect of live steam pressure on heat absorbed by steam plant, burner and stack temperatures: (a) Case A; (b) Case B.

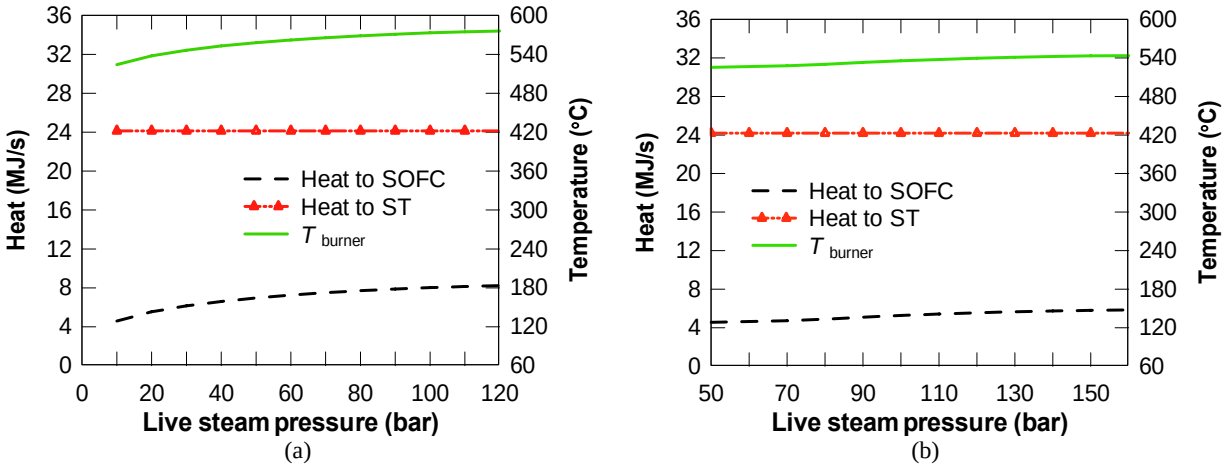

Fig. 8 Effect of live steam pressure on heat absorbed by steam plant, burner and stack temperatures: (a) Case C; (b) Case D.

recuperator decreased the exergy losses from the HRSG when live steam pressure was increased.

5. Summary

In Table 2, one can see the efficiency and power outputs of the different plant configurations discussed above. For the recuperated configurations 80 bars was selected as the highest pressure level in the steam cycle. The reason was basically on two important issues: available steam turbine at proposed size and steam temperature and, avoiding problems associated with designing and constructing the first row of the steam turbine when pressure is relatively high with relatively low mass flow. The dual pressure level with reheat had higher plant efficiency than the single pressure level, 0.628 respective 0.621. The hybrid recuperator increased the plant efficiency considerable both for single and dual pressure levels. This was possible by recovering more energy from the HRSG. However, the most interesting point was that the single pressure level with hybrid recuperator had higher plant efficiency than the dual pressure level with reheat, 0.682 and 0.667, respectively. It means that the energy recovery from the HRSG could be achieved more efficiently in the simple single pressure steam cycle than the dual pressure configuration. Note that the cost of a single pressure steam cycle is much lower than the dual pressure steam cycle with reheat. In other words, considerable energy recovery could be achieved with relatively low additional investment cost (by adding a single heat exchanger). Only one heat exchanger was added to the basic plant configuration, case A.

Table 2 Net powers and efficiencies of the plants suggested above.

Parameter	Case A	Case B	Case C	Case D
Live steam pressure (bar)	22	43	80	80
Net power output (MW)	37.01	37.41	40.60	39.80
Net power output from SOFC cycle (MW)	31.59	31.63	31.49	31.52
Net power output from ST cycle (MW)	5.42	5.78	9.11	8.28
Depleted gas temperature (°C)	191.1	173.1	90	90
Gas temperature before hybrid recuperator (°C)	-	-	210.6	167.0
Thermal efficiency of steam cycle (LHV)	0.308	0.307	0.377	0.343
Moisture content after ST (%)	11.5	12.2	14.5	11.9
Thermal efficiency of SOFC cycle (LHV)	0.530	0.531	0.468	0.489
Thermal efficiency of plant (LHV)	0.621	0.628	0.682	0.667

Case A: single pressure level, without hybrid recuperator;
Case B: dual pressure level, without hybrid recuperator;
Case C: single pressure level, with hybrid recuperator;
Case D: dual pressure level, with hybrid recuperator.

One could discuss that because the pressure was not optimal for the dual pressure level with hybrid recuperator (case D), therefore, the plant efficiency for the simple pressure level with hybrid recuperator (case C) showed larger plant efficiency. However, even if a pressure of 160 bars was chosen for the dual pressure with hybrid recuperator then the efficiency would be less than the simple pressure with recuperator at 80 bar (0.677 versus 0.682) as shown in Fig. 3. Thus, significant higher plant efficiency could be achieved with implementing a single heat exchanger without the need for dual pressure level in the bottoming cycle.

The off-gases from the HRSG maintained a high quality heat, which was used to preheat the air after the compressor in the SOFC cycle. This could be achieved because the SOFC plant was not pressurized and the temperature (as well as pressure) after the air compressor was low enough. The hybrid recuperator has two major impacts on the plant; more energy could be recovered from the HRSG, and since this energy was recycled back to the SOFC plant then more energy was available after the SOFC stacks. Having more energy after the SOFC stacks meant that more energy could be sent to the bottoming cycle which in turn could generate more power. In other words, both recovering and recycling could be achieved simultaneously. Note that in SOFC-GT-ST (SOFC-CC) hybrid plants, the SOFC plant is pressurized and consequently the temperature after the compressor is higher than the stack temperature and therefore a hybrid recuperator could not be used. In the dual pressure steam cycle, the off-gases have less energy to be utilized by hybrid recuperator and therefore the plant efficiency could not increase considerably compared to the single pressure steam cycle.

As was revealed form Table 2, for the cases without hybrid recuperator (case A and B), the dual pressure configuration could increase the plant efficiency compared to the simple pressure level, as expected. The major reason was that the bottoming cycle could generate more power in the dual pressure configuration (360 kW additional), with relatively unchanged steam cycle efficiency (30.7% versus 30.8%).

Another interesting point was that for the cases with hybrid recuperator (case C and D), the topping cycle efficiency was lower in the simple pressure configuration than the dual pressure configuration. This was happened despite the fact that the plant efficiency was higher in the simple pressure configuration than the dual pressure configuration.

The major explanation for such occurrence was the efficiency definition expressed in Eq. (22). In the

simple pressure configuration (case C) more heat was available for recycling it back to the topping cycle than the dual pressure configuration (case D), compare 210.6 °C with 167 °C which were the off-gases temperatures before hybrid recuperator. Furthermore, the net power generated by the topping cycle remained almost unchanged. The small increase in the net power generated by the topping cycle, (both recuperated cases compared to non-recuperated cases), was due to additional mass flow of compressor to compensate the additional pressure drop in the heat exchangers. This resulted that more heat could be removed from the SOFC stacks which in turn allowed for additional generated power.

6. Conclusions

A hybrid combined SOFC-ST plant was presented and analyzed with firstly a single pressure steam cycle and secondly a dual pressure steam cycle with reheat and preheat. Unlike many previous studies, the SOFC plant presented here in hybrid SOFC-ST mode was not pressurized. The plant was fired by natural gas, and therefore the fuel was desulfurized before sending it to the pre-reformer reactor. An adiabatic steam reformer was used to pre-process the fuel before sending it to the anode side of the SOFC stacks.

For the non-hybrid recuperation cases it was shown that SOFC-ST with a dual pressure steam cycle with reheat and pre-heater was superior to the single pressure steam cycle. This was in accordance to the traditional CC cycles wherein dual pressure level steam cycles have a higher efficiency than the single pressure steam cycles. The achieved plant efficiency was 62.1% versus 62.8%.

For the hybrid recuperation cases the situation was reversed. It was shown that SOFC-ST with a single pressure level had a higher plant efficiency and net power output than the dual pressure configuration. The reason was that more energy could be recovered from the HRSG in this case. The plant efficiency was 68.2% for the single pressure configuration while it was 66.7% for the dual pressure configuration.

Furthermore, it was also determined that the hybrid recuperator could increase the plant efficiency significantly regardless if a single pressure or dual pressure steam cycle was used as a bottoming cycle. The increase efficiency was 6.1 point percentage for the single pressure while it was 3.9 point percentage for the dual pressure steam cycle. Such improvement plant efficiency could be achieved by adding only one heat exchanger. Thus, it was concluded that in order to increase the efficiency of the SOFC-ST hybrid plants, it was enough to use a single heat exchanger (as hybrid recuperator) without increasing the pressure levels in the steam cycle. This was an important conclusion since the implementing one heat exchanger is significantly less costly than a dual or triple pressure level in the steam cycle.

Finally, by applying a hybrid recuperator the duty of the cathode pre-heater will be decreased which in turn decreases its cost proportionally.

References

[1] E. Fontell, T. Kivisaari, N. Christiansen, J.B. Hansen, J. Pålsson, Conceptional study of a 250 kW planar SOFC system for CHP application, J. Power Sources 131 (2004) 49-56.

[2] M. Rokni, Introduction of a fuel cell into combined cycle: A competitive choice for future cogeneration, in: 7th Congress & Exposition on Gas Turbines in Cogeneration and Utility Industrial and Independent Power Generation, Bournemouth, UK, 1993.

[3] E. Riensche, E. Achenbach, D. Froning, M.R. Haines, W.K. Heidug, A. Lokurlu, et al., Clean combined-cycle SOFC power plant—Cell modeling and process analysis, J. Power Sources 86 (2000) 404-410.

[4] J. Pålsson, A. Selimovic, L. Sjunnesson, Combined solid oxide fuel cell and gas turbine systems for efficient power and heat generation, J. Power Sources 86 (2000) 442-448.

[5] T. Proell, C. Aichering, R. Rauch, H. Hofbauer, Coupling of biomass steam gasification and an SOFC-gas turbine hybrid system for highly efficient electricity generation, in: ASME Turbo Expo, Vienna, Austria, June 14-17, 2004, pp. 103-112.

[6] C. Bang-Møller, M. Rokni, Thermodynamic performance study on biomass gasification, solid oxide fuel cell and micro gas turbine hybrid systems, Energy Conversion and Management 51 (2010) 2330-2339.

[7] K. Subramanyan, U.M. Diwekar, Characterization and quantification of uncertainty in solid oxide fuel cell hybrid power plants, J. Power Sources 142 (2005) 103-116.

[8] F. Calise, D.M. d'Accadia, L. Vanoli, M.R. von Spakovsky, Single-level optimization of hybrid SOFC-GT power plant, J. Power Sources 159 (2006) 1169-1185.

[9] C. Wächter, R. Lunderstädt, F. Joos, Dynamic model of a pressurized SOFC/gas turbine hybrid power plant for the development of control concept, J. Fuel Cell Science and Technology 3 (2006) 271-279.

[10] R.A. Roberts, J. Brouwer, Dynamic simulation of a pressurized 220 kW solid oxide fuel-cell-gas-turbine hybrid system: Modeled performance compared to measured results, J. Fuel Cell Science and Technology 3 (2006) 18-25.

[11] M. Rokni, E. Fontell, Y. Ylijoki, O. Tiihonen, M. Hänninen, Dynamic modeling of Wärtsilä 5 kW SOFC system, in: Ninth International Symposium on Solid Oxide Fuel cell, Quebec, Canada, 2005.

[12] P. Costamagna, L. Magistri, A.F. Massardo, Design and part-load performance of a hybrid system based on a solid oxide fuel cell reactor and a micro gas turbine, J. Power Sources 96 (2001) 352-368.

[13] W.R. Dunbar, N. Lior, R.A. Gaggioli, Combining fuel cells with fuel-fired power plants for improved exergy efficiency, J. Energy 16 (1991) 1259-1274.

[14] M. Rokni, Thermodynamic analysis of an integrated solid oxide fuel cell cycle with a Rankine cycle, J. Energy Conversion and Management 51 (2010) 2724-2732.

[15] M. Rokni, Thermodynamic analysis of an integrated gasification plant with solid oxide fuel cell cycle and steam cycle, J. Green 2 (2012) 71-86.

[16] B. Elmegaard, N. Houbak, DNA—A general energy system simulation tool, in: Proceeding of SIMS 2005, Trondheim, Norway, 2005.

[17] C. Perstrup, Analysis of power plant installation based on network theory, M.Sc. Thesis, Laboratory of Energetics, Technical University of Denmark, 1989. (in Danish)

[18] T.F. Petersen, N. Houbak, B. Elmegaard, A zero-dimensional model of a 2ND generation planar SOFC with calibrated parameters, Int. J. Thermodynamics 9 (2006) 161-169.

[19] P. Holtappels, L.G.J. DeHaart, U. Stimming, I.C. Vinke, M. Mogensen, Reaction of CO/CO_2 gas mixtures on Ni-YSZ cermet electrode, J. Appl. Electrochem. 29 (1999) 561-568.

[20] Y. Matsuzaki, I. Yasuda, Electrochemical oxidation of H_2 and CO in a H_2-H_2O-CO-CO_2 system at the interface of a Ni-YSZ cermet electrode and YSZ electrolyte, Electrochem. Soc. 147 (2000) 1630-1635.

[21] K.M. Keegan, M. Khaleel, L.A. Chick, K. Recknagle, S.P. Simner, J. Diebler, Analysis of a planar solid oxide fuel cell based automotive auxiliary power unit, SAE Technical Paper [Online], Mar. 4, 2002, http://papers.sae.org/2002-01-0413/.

[22] J.W. Kim, A.V. Virkar, The effect of anode thickness on the performance of anode-supported solid oxide fuel cell, in: Proc. of the Sixth Int. Symp. on SOFCs-(SOFC-VI), PV99-19, Honolulu, Hawaii, Oct. 17-22, 1999, pp. 830-839.

[23] J.M. Smith, H.C. van Ness, M.M. Abbott, Introduction to Chemical Engineering Thermodynamics, 7th ed., McGraw-Hill, Boston, 2005.

[24] J. Winnick, Chemical Engineering Thermodynamics, John Wiley & Sons, New York, 1997.

[25] R.H. Kehlhofer, J. Warner, H. Nielsen, R. Bachmann, Combined-Cycle Gas Steam Turbine Power Plants, 2nd ed., PennWell, Oklahoma, 1999.